Microstructure and mechanical properties of $Al_2O_3/Er_3Al_5O_{12}$ eutectic rods grown by the laser-heated floating zone method

M.C. Mesa [a], P.B. Oliete [a,*], V.M. Orera [a], J.Y. Pastor [b], A. Martín [b], J. LLorca [c]

[a] *Instituto de Ciencia de Materiales de Aragón, CSIC–Universidad de Zaragoza, María de Luna 3, 50018 Zaragoza, Spain*
[b] *Departamento de Ciencia de Materiales, Universidad Politécnica de Madrid, E.T.S. de Ingenieros de Caminos, E28040 Madrid, Spain*
[c] *Departamento de Ciencia de Materiales, Universidad Politécnica de Madrid & Instituto Madrileño de Estudios Avanzados de Materiales (IMDEA-Materiales), E.T.S. de Ingenieros de Caminos, E28040 Madrid, Spain*

Abstract

Eutectic rods of Al_2O_3–$Er_3Al_5O_{12}$ were grown by directional solidification using the laser-heated floating zone method at rates in the range 25–1500 mm/h. Their microstructure and mechanical properties (hardness, toughness and strength) were investigated as a function of the growth rate. A homogeneous and interpenetrated microstructure was found in most cases, and interphase spacing decreased with growth rate following the Hunt–Jackson law. Hardness increased slightly as the interphase spacing decreased while toughness was low and independent of the microstructure. The rods presented very high bending strength as a result of the homogeneous microstructure, and their strength increased rapidly as the interphase spacing decreased, reaching a maximum of 2.7 GPa for the rods grown at 750 mm/h. The bending strength remained constant up to 1300 K and decreased above this temperature. The relationship between the microstructure and the mechanical properties was established from the analysis of the microstructure and of the fracture mechanisms.

Keywords: Microstructure; Mechanical properties; High temperature; Al_2O_3–$Er_3Al_5O_{12}$; Directionally solidified eutectic oxides

1. Introduction

Directionally solidified eutectic oxides (DSEO) have attracted a great deal of interest over recent decades because of their outstanding properties derived from their unique microstructure.[1] Among them, DSEO based on Al_2O_3 stand out because of their high strength retention at high temperature and creep resistance, in addition to their unpaired microstructural stability and degradation resistance in atmospheric oxidizing environments at temperatures near the eutectic temperature. These properties make this material a promising candidate as a high-temperature structural material[1,2] and binary and ternary eutectics of the Al_2O_3–ZrO_2–Y_2O_3 system have been extensively studied in the past. Excellent mechanical properties were reported on both binary Al_2O_3–$Y_3Al_5O_{12}$[3–5] and ternary Al_2O_3–$Y_3Al_5O_{12}$–ZrO_2 eutectics,[6] reaching a room temperature bending strength close to 5 GPa.[7]

More recent research activities were focussed on the development of new DSEO incorporating other promising ceramic oxides.[8–10] For example, the addition of rare earth oxides to the eutectic composition may prove to be of interest as rare earth ions in crystals at high-temperature emit radiation in narrow bands, allowing their use as selective emitters.[11] Particularly, a strong selective emission band due to the Er^{3+} ion in the Al_2O_3–$Er_3Al_5O_{12}$ eutectic matches up with the sensitive region of a GaSb photovoltaic cell,[12] allowing the application field of these eutectics to be extended. Binary and ternary eutectic studies of the Al_2O_3–ZrO_2–Er_2O_3 system have recently been reported[12–14] but experimental results on the mechanical properties of this material are still very limited.

The aim of this paper is to understand the relationship between the microstructure and the mechanical properties of Al_2O_3–Er_2O_3 eutectic rods, so that the influence of the growth conditions on material performance can be established. DSEO rods were grown using the laser-heated floating zone method (LHFZ). Among the different directional solidification techniques to grow ceramic eutectics, the LHFZ method does not require a crucible and provides very large thermal gradients at the liquid/solid interface, which allows the use of high growth

rates. Hence, crystals with different microstructure can be grown by changing the growth parameters. The mechanical properties (hardness, toughness, and strength) of Al_2O_3–Er_2O_3 eutectic rods with different microstructure were measured at 300 K and, in addition, their bending strength in air was measured up to 1900 K. The results of the mechanical tests, together with the analysis of fracture micromechanisms, were used to ascertain the factors that controlled the mechanical properties of Al_2O_3–$Er_3Al_5O_{12}$ eutectic materials as a function of microstructure and temperature.

2. Materials and experimental techniques

Eutectic rods of Al_2O_3–$Er_3Al_5O_{12}$ were prepared by the LHFZ technique, according to the following process: (i) ceramics were prepared using a mixture of commercial powders of Er_2O_3 (Aldrich, 99%) and Al_2O_3 (Aldrich, 99.99%) with the eutectic composition (81 mol% Al_2O_3, 19 mol% Er_2O_3).[15] (ii) Al_2O_3 powders were milled using a vibratory mill (model MM20000, Restch, Haan, Germany) and fired in air at 1000 °C for 1 h. (iii) Precursor rods were prepared by isostatic pressing of the powder for 3 min at 200 MPa. (iv) The rods obtained were sintered in a furnace at 1500 °C for 12 h. The final precursor rods had a typical diameter of 2.5 mm.

Eutectic rods were obtained by directional solidification of the precursors by the LHFZ method using a CO_2 laser in nitrogen atmosphere, with a slight overpressure of 0.1–0.25 bar with respect to ambient pressure, to avoid the appearance of gas inclusions in the solidified rod.[16] Growth rates in the range 25–1500 mm/h were used to develop materials with different microstructure. Several densification stages were applied at low growth rates (100–250 mm/h) in order to avoid precursor porosity. The last stage was always performed with the solidified rod travelling downwards and without rotation of the crystal and precursor. The crystals presented a nominal final diameter in the range 1–1.5 mm.

Transverse and longitudinal cross-sections of the grown rods were cut and polished for scanning electron microscopy analysis. The microstructure was studied using the back-scattered electron images obtained in a scanning electron microscope (model 6400, Jeol, Tokyo, Japan). In addition, the hydrostatic component of the alumina stress tensor was locally determined by means of the Cr^{3+} luminescence of residual chromium impurities using piezo-spectroscopic methods. Piezo-spectroscopic measurements were performed by using an optical spectrometer (Model XY, DILOR, Lille, France). The ruby luminescence was excited with the 514.5 nm line of an Ar^+-ion laser and collected at room temperature using a triple 0.5 m monochromator with CCD detector coupled to an optical microscope with spectral resolution of 0.3 cm^{-1}. The luminescence was measured using a micro-Raman facility in the backscattering configuration and a long focal length microscope objective of 50×. In these conditions the lateral resolution is about 2 μm and the diffuse light beam penetrates more than 20 μm depth into the sample giving a bulk measurement of the stresses. The luminescence bands were corrected against the 14,431 cm^{-1} line of a neon discharge lamp.

The Vickers hardness was measured following the ASTM C1327-99 Standard using a Matsuzawa, MXT 70 microhardness tester. An indentation load of 4.9 N and a holding time of 15 s were used for these measurements. No less than 10 valid indentations were made on polished transverse cross-sections of each sample. The fracture toughness was determined by the indentation technique. The crack lengths were measured using the optical microscope of the microhardness tester. The dynamic elastic modulus of the rods in the longitudinal direction was determined by the flexural vibration resonance method on rods of 30 mm in length (Grindosonic MK4i, J.W. Lemmens, Belgium).

The bending strength of the rods at room temperature was determined from three-point flexural tests performed in air in a servomechanical testing machine (model 4505 Instron Ltd., UK) with an 8.5 mm loading span and a crosshead speed of 100 μm/min. A minimum of three tests were performed on each test condition. The specimen and the loading fixture were placed in a furnace and loaded through two alumina rods connected to the actuator and load cell, respectively, for the high-temperature tests. The heating rate was 10 K/min up to 1300 K, 5 K/min up to 1500 K, 3 K/ min up to 1750 K, and 1 K/min above this point. The specimen was held at the test temperature for 30 min before testing. All tested samples showed linear load–displacement behavior and so the strength was calculated from the maximum load in the test using the standard beam theory.

3. Results and discussion

3.1. Microstructure

Samples grown at growth rates of 25, 350 and 750 mm/h were found to be free of voids and cracks and presented a homogeneous microstructure throughout the entire cross-section of the grown rod. Scanning electron micrographs showing the microstructure of the transverse cross-section of the samples grown at 25, 350 and 750 mm/h are shown in Fig. 1(a)–(c), respectively. A three-dimensional interpenetrating network of Al_2O_3 (black contrast) and $Er_3Al_5O_{12}$ (white contrast), commonly referred to as Chinese Script microstructure, was observed for all the growth rates. The microstructure showed an alignment of the elongated eutectic phases along the growth direction for all the solidification rates (Fig. 1d), as usually occurs in directionally solidified eutectics. The tendency of the component phases to develop facets (Fig. 1a) was evident at low growth rates, as a result of their high entropy of melting (48 J/K mol for Al_2O_3 and 122 J/K mol for $Y_3Al_5O_{12}$, which is expected to be very close to that of $Er_3Al_5O_{12}$).[17,18] Obviously, a phase size refinement was found with increasing growth rate. Similar microstructures have been observed previously in other Al_2O_3-based DSEO, such as Al_2O_3–$Y_3Al_5O_{12}$,[4] and Al_2O_3–$GdAlO_3$.[19] The $Er_3Al_5O_{12}$ volume fraction estimated from the area fraction in micrographs was 53.5 ± 2.5%, in agreement with the value of 56% calculated from the eutectic composition.

Rods grown at rates higher than 750 mm/h incorporated some gas bubbles in the centre of the rods. These bubbles covered

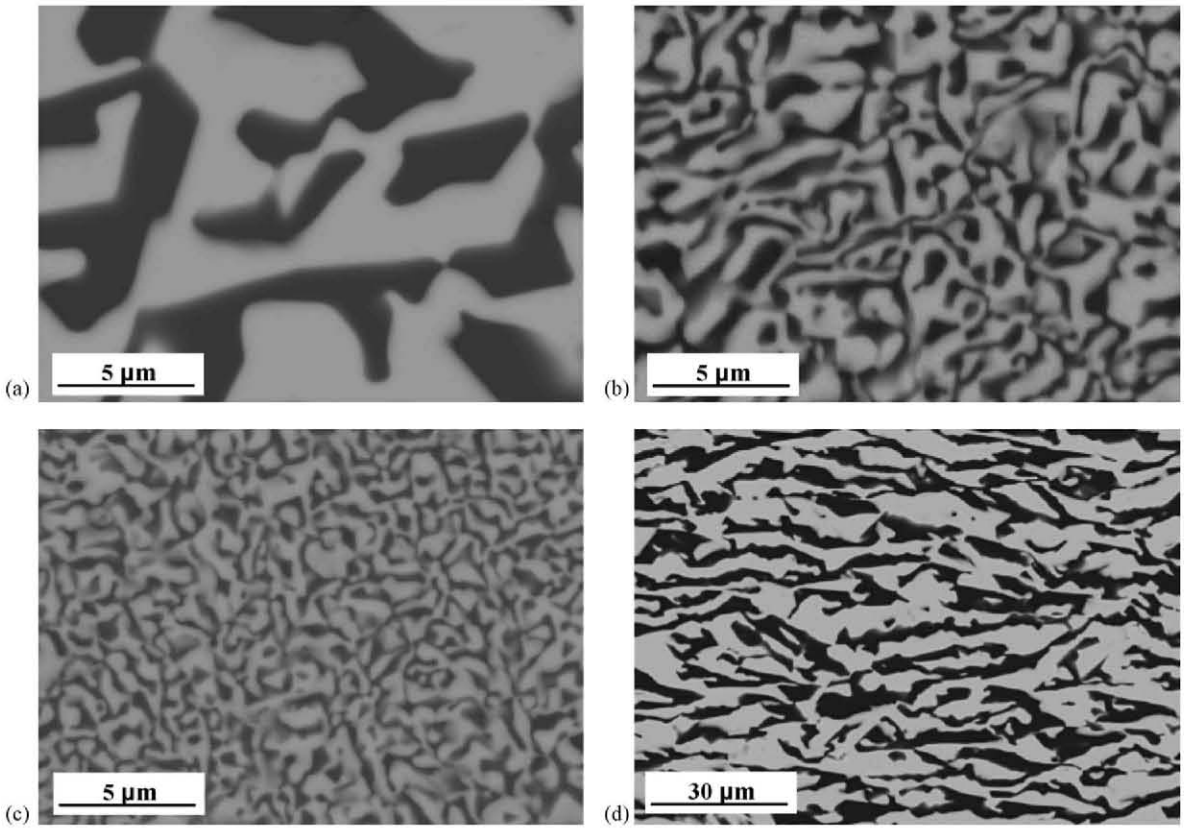

Fig. 1. Back-scattered scanning electron micrographs of the transverse cross-section of Al_2O_3–$Er_3Al_5O_{12}$ eutectic rods grown at various rates, (a) 25 mm/h (b) 350 mm/h and (c) 750 mm/h. (d) Longitudinal cross-section of Al_2O_3–$Er_3Al_5O_{12}$ eutectic rods grown at 25 mm/h. Al_2O_3 is the dark phase.

<2% of the surface in both transverse and longitudinal sections. The presence of voids at high growth rates has been previously reported in other Al_2O_3-based eutectics and has been attributed to the existence of gas dissolved in the melt.[20] Since the solubility of a gas in a solid is generally smaller than in a liquid, gas bubbles can be nucleated during solidification due to the gas rejected into the melt.[20] When the solidification rates used in the growth are low, the gas is permitted to diffuse away from the solid–liquid interface. However, at high growth rates, gas concentration raises and bubbles nucleated in the solid–liquid interface are entrapped in the solid.[16,20] The volume fraction of pores was observed to increase with the oxygen partial pressure of the processing atmosphere and the use of non-oxidant growth atmospheres produced a large reduction in the gas entrapment.[16] A nitrogen atmosphere was used for the growth of the rods studied in this work which reduced the bubbles present in the samples at a very low level, even for the samples grown at 1500 mm/h with a void surface ratio of ~1.5%.

In addition to the small amount of gas inclusions, the samples grown at 1200 and 1500 mm/h presented a non-homogeneous microstructure. Regions with an interpenetrating microstructure (as presented in Fig. 1) were mixed with regions with a fibrous pattern. Fig. 2(a) and (b) presents two scanning electron micrographs of both arrangements corresponding to the longitudinal cross-section of rods grown at 1200 mm/h. This transition from a homogeneous Chinese Script microstructure to a mixed interpenetrated-fibrous pattern has been observed previously in the directionally solidified $Al_2O_3/GdAlO_3$ eutectic.[8,19] The microstructure change may be due to the fact that the tendency to develop facets is reduced as the solidification rate is raised, leading to a more regular morphology.[21]

As is well known, if the diffusion distance in the liquid is larger than the eutectic spacing, the system fulfils the Hunt–Jackson condition and the interspacing λ depends on the growth rate v according to the Hunt–Jackson law[22]:

$$\lambda^2 v = C \tag{1}$$

where C is a constant which depends essentially on the phase diagram and the diffusion coefficient of the ions in the melt.[1,22] The interphase spacing, λ, was determined by linear analysis of cross-section micrographs obtained in the scanning electron microscope. The evolution of λ as a function of the growth rate v is plotted in Fig. 3. As expected, the higher the growth rate the finer the microstructure, and the interlamellar distance decreased to values as low as 300 nm for growth rates of 1500 mm/h. Average interphase spacing was accurately predicted by Eq. (1) with $C = 135\ \mu m^3/s$. This is slightly higher than the value of $\sim 100\ \mu m^3/s$ determined for Al_2O_3–YAG eutectics.[16,23]

3.2. Residual stresses

Due to the differences in the thermal expansion coefficients and to the strong interfacial bonding between the phases, residual stresses develop when the eutectic is cooled down from the melt

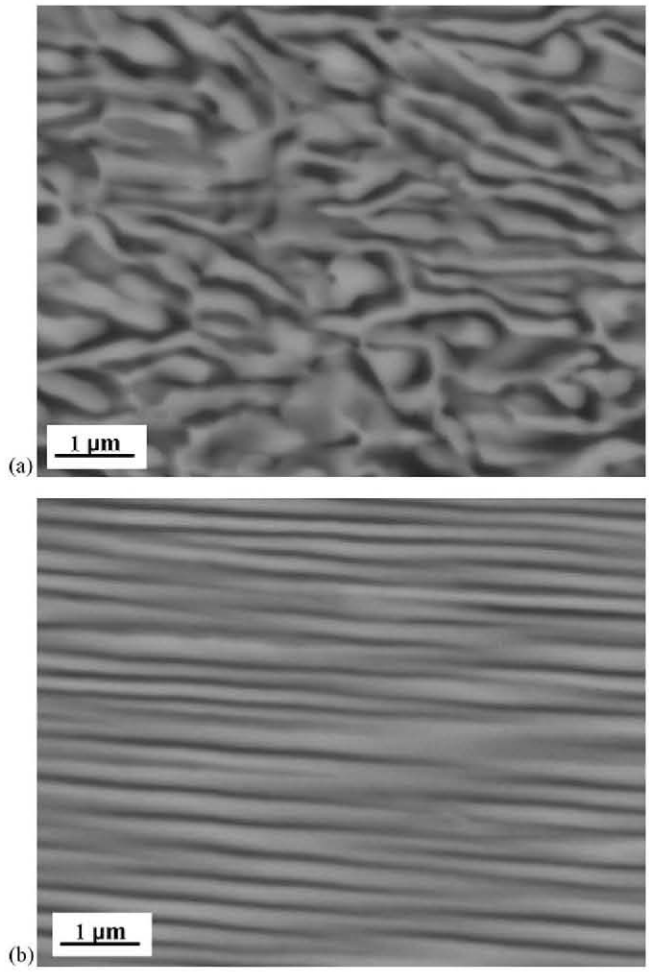

Fig. 2. Back-scattered scanning electron micrographs of the longitudinal cross-section of Al_2O_3–$Er_3Al_5O_{12}$ eutectic rods grown at 1200 mm/h. (a) Interpenetrated microstructure and (b) fibrilar pattern.

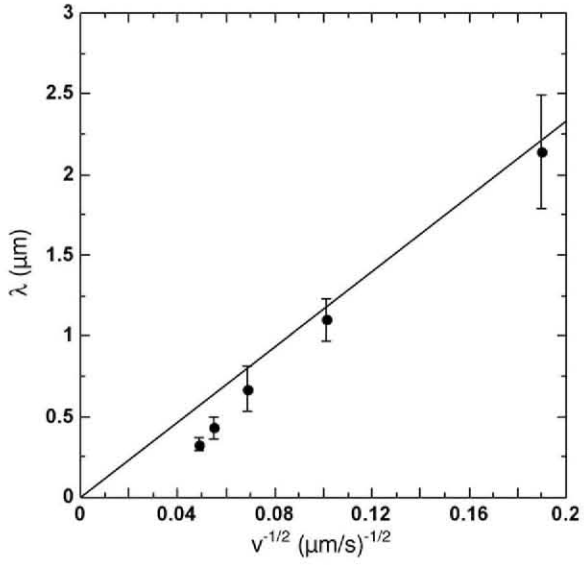

Fig. 3. Evolution of lamellar interspacing, λ, with the growth rate, v, for Al_2O_3–$Er_3Al_5O_{12}$ eutectic rods. Solid circles correspond to the experimental values and the line corresponds to the fitting to the Hunt–Jackson law with $C = 135\ \mu m^3\ s^{-1}$.

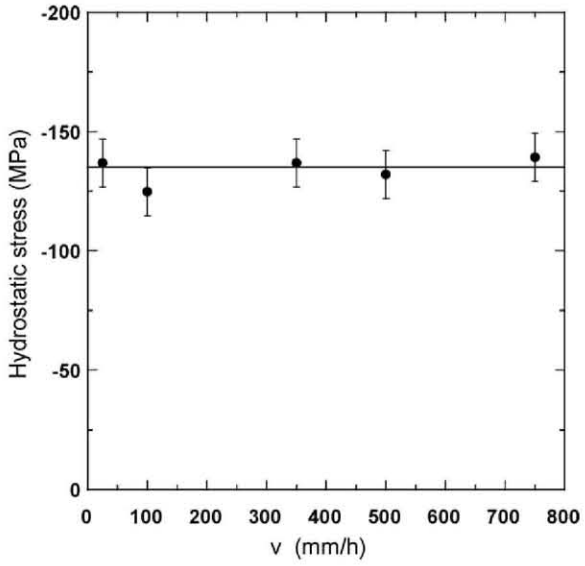

Fig. 4. Hydrostatic residual stresses in the Al_2O_3 phase measured on Al_2O_3–$Er_3Al_5O_{12}$ eutectic rods as a function of the growth rate.

up to room temperature. Residual stresses may have a strong influence on the mechanical behavior of the eutectic.[1,24]

The hydrostatic component of the residual stresses in the Al_2O_3 phase was determined by means of the spectroscopic effect of the ruby R emission lines in the eutectic rods. At 297 K the unstressed ruby luminescence spectrum consists of the R1 and R2 lines, at 14,403 and 14,433 cm^{-1} and halfwidths of 11.25 and 8.8 cm^{-1}, respectively, associated to the $E(^2E) \rightarrow {}^4A_2$ and $^2A(^2E) \rightarrow {}^4A_2$ transitions of the $Cr^{3+}(d^3)$, respectively. Since the peak positions of the R-lines depend to a large extent on the Cr^{3+} environment, the relationship between the R-line shifts and stress has been used for pressure calibration in high pressure devices and to determine with high spatial resolution, the residual stresses in Al_2O_3-based materials.[25,26] In addition, the R2-line position is rather insensitive to the non-hydrostatic strain components.[27] R2-line shifts $\Delta\nu_2$ were determined with respect to that of a Al_2O_3:Cr^{3+} (0.11 wt% Cr_2O_3) single crystal. An analysis of the band shapes was performed in order to obtain quantitative values of the peak positions, ν_c and the full widths at half maximum w_L. The shape of the bands was approximated by two single Lorentzian curves, $y(\nu) = y_0 L(\nu - \nu_c, w_L)$, leaving ν_c and w_L as fitting parameters.

The hydrostatic component σ_h^A (in GPa) of the residual stresses in the alumina phase can be calculated using the following scalar relationship[28]:

$$\sigma_h^A = \frac{\Delta\nu_2}{7.61} \tag{2}$$

Fig. 4 shows the magnitude of σ_h^A, which was independent of the growth rate and thus of the phase size since the volume fraction of both phases remained constant. Sapphire was subjected to a compressive stress of ≈ -135 MPa. A theoretical estimation of the thermo-elastic residual stresses can be obtained using the self-consistent approximation, as presented in [29] from the elastic constants, thermal expansion coefficients and volume fraction of both phases in the eutectic. The thermo-elastic constants of

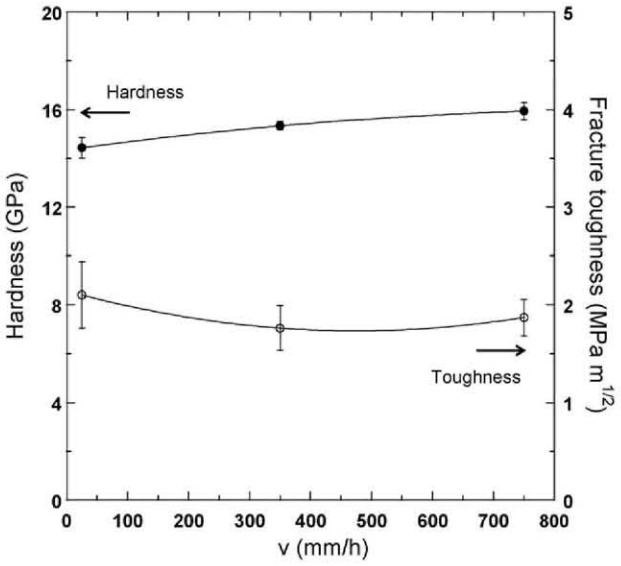

Fig. 5. Microhardness and fracture toughness of Al_2O_3–$Er_3Al_5O_{12}$ eutectic rods as a function of the growth rate.

Al_2O_3 can be found in [29], as well as the elastic modulus of $Y_3Al_5O_{12}$, which was used instead of that $Er_3Al_5O_{12}$. The thermal expansion coefficient of $Er_3Al_5O_{12}$ is $9 \times 10^{-6}\,K^{-1}$ according to Ovanesyan.[30] Assuming a stress-free temperature of 1273 K, the self-consistent model predicts a hydrostatic residual stress of −115 MPa in the Al_2O_3 at room temperature, which is in good agreement with the experimental results. This coincidence is in favour of the absence of stress relaxation mechanisms such as interface decohesion or microcracking upon cooling.

3.3. Mechanical behaviour

Rods with homogeneous microstructure and free of voids grown at 25, 350 and 750 mm/h were used for the characterization of mechanical properties.

3.3.1. Microhardness and fracture toughness

Hardness and fracture toughness of the eutectic rods were determined from Vickers microhardness tests at room temperature. Fig. 5 shows the average microhardnesses measured on the transverse cross-section of Al_2O_3–$Er_3Al_5O_{12}$ eutectic rods grown at 25, 350 and 750 mm/h. They were in the range 14.5–16 GPa, and these values were very close to those measured by Pastor et al.[4] and Larrea et al.[31] in directionally solidified Al_2O_3–$Y_3Al_5O_{12}$ eutectics, corroborating the fact that hardness in DSE oxides is mainly a function of that of constituent phases. The hardness was observed to increase very slightly with growth rate as the microstructure becomes finer. A similar dependence of the hardness with the growth rate has been previously reported by several authors in other Al_2O_3-based DSE.[4,6,32] This increase of microhardness for finer microstructures can be attributed to the strengthening effect of the strong interfaces between Al_2O_3 and $Er_3Al_5O_{12}$, which limits the microplastic deformation around the indentation.

Fracture toughness was determined from the length of the cracks caused from the Vickers indentations. Although the indentation method is not considered appropriate for the absolute determination of fracture toughness,[33,34] it is adequate to compare the values obtained from samples grown at different rates,[31,35] and to provide an estimation of the fracture toughness. Fig. 6(a) presents the indentation fracture pattern showing symmetric and well-defined cracks. Crack propagation was transgranular and no crack deflection was observed at the interfaces between Al_2O_3 and $Er_3Al_5O_{12}$ (Fig. 6(b)). This brittle behavior is a consequence of the strong bonding between the eutectic phases and of the low thermo-elastic residual stresses. K_{IC} was determined using the equation proposed by Anstis[36] for median cracks,

$$K_{IC} = 0.016\left(\frac{E}{H}\right)^{1/2}\left(\frac{P}{c^{3/2}}\right) \tag{3}$$

where P is the indentation load, c the distance from the centre of the indentation to the crack tip and E the Young modulus of the eutectic (=311 GPa), obtained by the flexural vibration resonance method, which was independent of the growth rate. Typical c values for all the samples were 30 μm, which fulfilled the Niihara condition[37] for median cracks ($c/a > 2.5$), where a stands for the half diagonal of the Vickers indentation. Fig. 5 shows the average values of the fracture toughness,

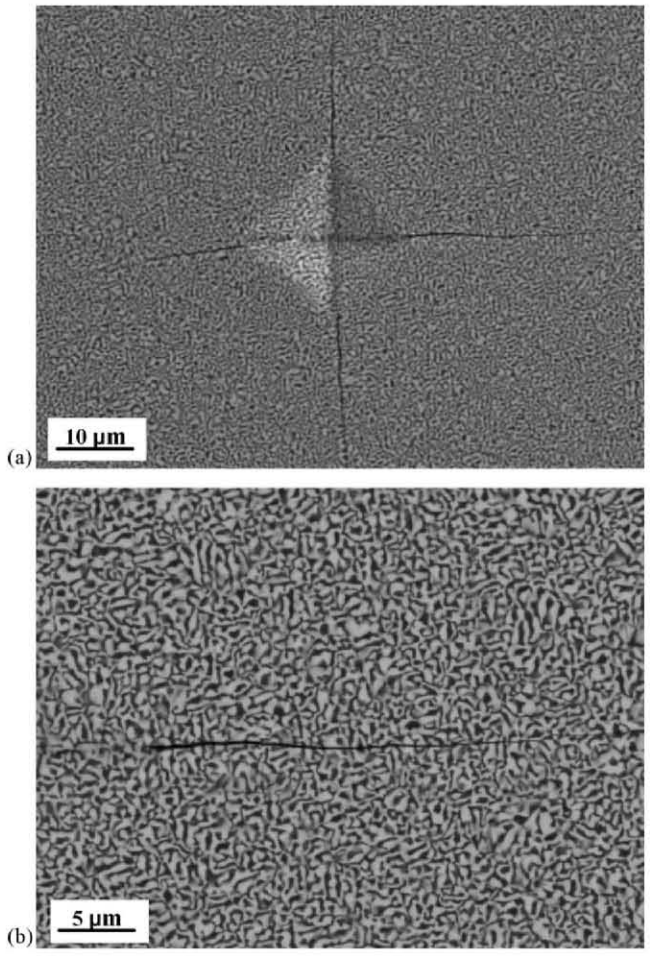

Fig. 6. (a) Cracking pattern and (b) crack propagation detail of the Al_2O_3–$Er_3Al_5O_{12}$ eutectic rod grown at 750 mm/h under an indentation load of 4.9 N.

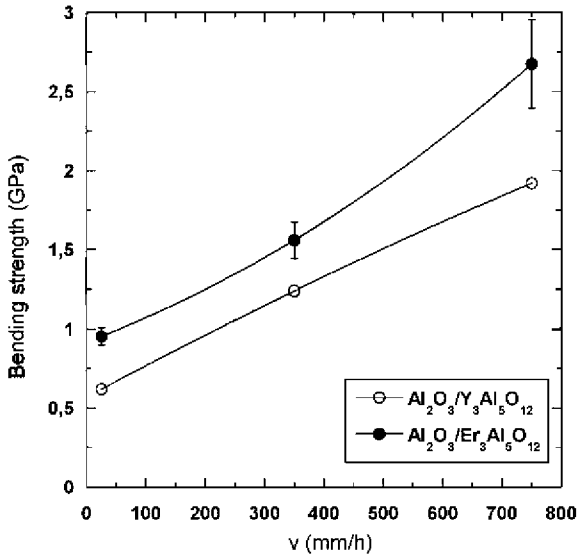

Fig. 7. Bending strength at room temperature of Al_2O_3–$Er_3Al_5O_{12}$ eutectic rods as a function of growth rate. The experimental results for Al_2O_3–$Y_3Al_5O_{12}$ eutectic rods in [4] are also shown for comparison.

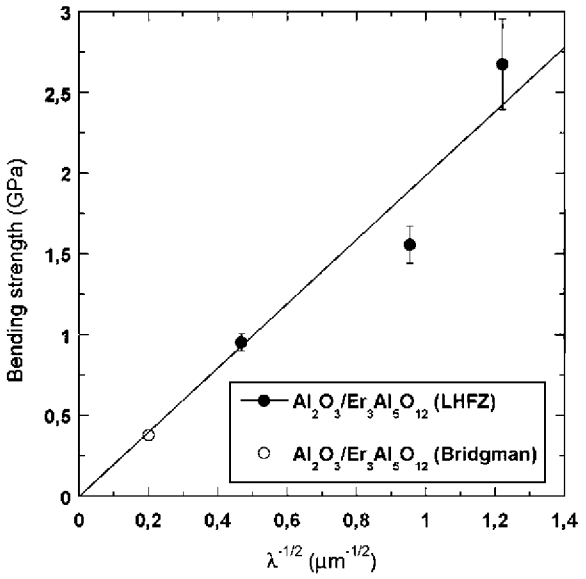

Fig. 8. Bending strength of Al_2O_3–$Er_3Al_5O_{12}$ eutectic rods grown by the LHFZ method as a function of lamellar interspacing. The experimental result Waku et al.[39] for rods grown using the Bridgman method is also included. The line corresponds to the predictions of Eq. (3) with $K_{IC} = 2.3$ MPa m$^{1/2}$.

determined from Eq. (3), as a function of growth rate. No a clear dependence on the rate was observed, with a mean value for K_{IC} of 1.9 MPa m$^{1/2}$, in agreement with the results obtained for Al_2O_3–$Y_3Al_5O_{12}$ eutectic rods grown using different melt-grown techniques.[4,38]

3.3.2. *Bending strength*

Three-point bending tests were performed on samples grown at 25, 350 and 750 mm/h from room temperature up to 1900 K to study the evolution of the mechanical properties of the Al_2O_3–$Er_3Al_5O_{12}$ eutectic rods with temperature. Fig. 7 shows the average bending strength, σ_f, (together with the corresponding standard error) as a function of the growth rate at room temperature. The bending strength of directionally solidified Al_2O_3–$Y_3Al_5O_{12}$ eutectic rods[4] is also presented for comparison. An increase of the bending strength in Al_2O_3–$Er_3Al_5O_{12}$ eutectic rods with respect to Al_2O_3–$Y_3Al_5O_{12}$ eutectic strength is clearly observed. While the hardness and the toughness of the Al_2O_3–$Er_3Al_5O_{12}$ eutectic rods were not affected by the growth rate, the bending strength increased sharply as the growth rate increased from 0.9 GPa at 25 mm/h to 2.7 GPa at 750 mm/h. This latter value was seven times higher than that of 380 MPa previously reported in the literature for this eutectic.[12,39]

The dependence of bending strength on growth rate, that is, on phase size, can be explained by taking into account that the strength of any brittle ceramic is controlled by the size of surface defects and the resistance to crack propagation. Assuming that the surface defects leading to fracture behave as semicircular cracks, flexural strength can be expressed as a function of fracture toughness, K_{IC}, and critical defect size, a_c, by the expression[4,40]:

$$\sigma_f = \left[\frac{K_{IC}}{0.65 \cdot \sqrt{\pi}}\right] \frac{1}{\sqrt{a_c}} \qquad (4)$$

In order to show whether the size of the strength-limiting flaw correlates with the eutectic spacing in the directionally solidified Al_2O_3–$Er_3Al_5O_{12}$ eutectic, the bending strength was plotted as a function of the interspacing λ in Fig. 8. A linear dependence of σ_f with $\lambda^{-1/2}$ was found, in agreement with Eq. (4). The value of the fracture toughness determined by fitting Eq. (4) to the experimental values (solid line in the figure), was 2.3 MPa m$^{1/2}$, very close to the experimental value of 1.9 MPa m$^{1/2}$ measured by the indentation technique. The bending strength reported by Waku et al.[39] in Al_2O_3–$Er_3Al_5O_{12}$ eutectic grown by Bridgman technique at 5 mm/h is included in Fig. 8, and very accurately follows the functional dependence of σ_f with λ established in Eq. (4).

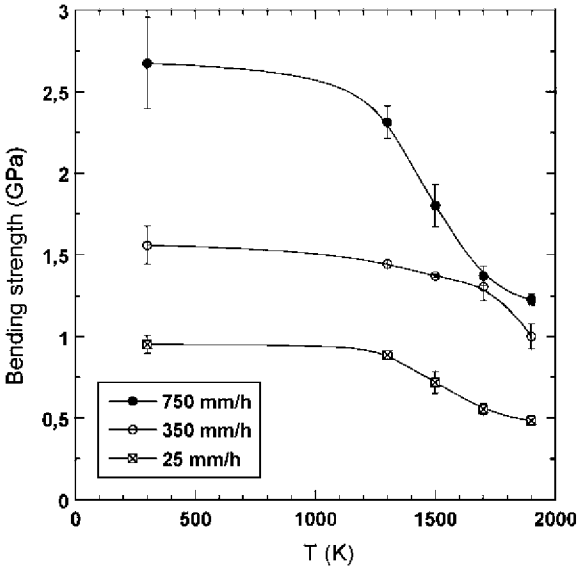

Fig. 9. Bending strength of Al_2O_3–$Er_3Al_5O_{12}$ eutectic rods grown at 25 mm/h, 350 mm/h and 750 mm/h rates as a function of the temperature.

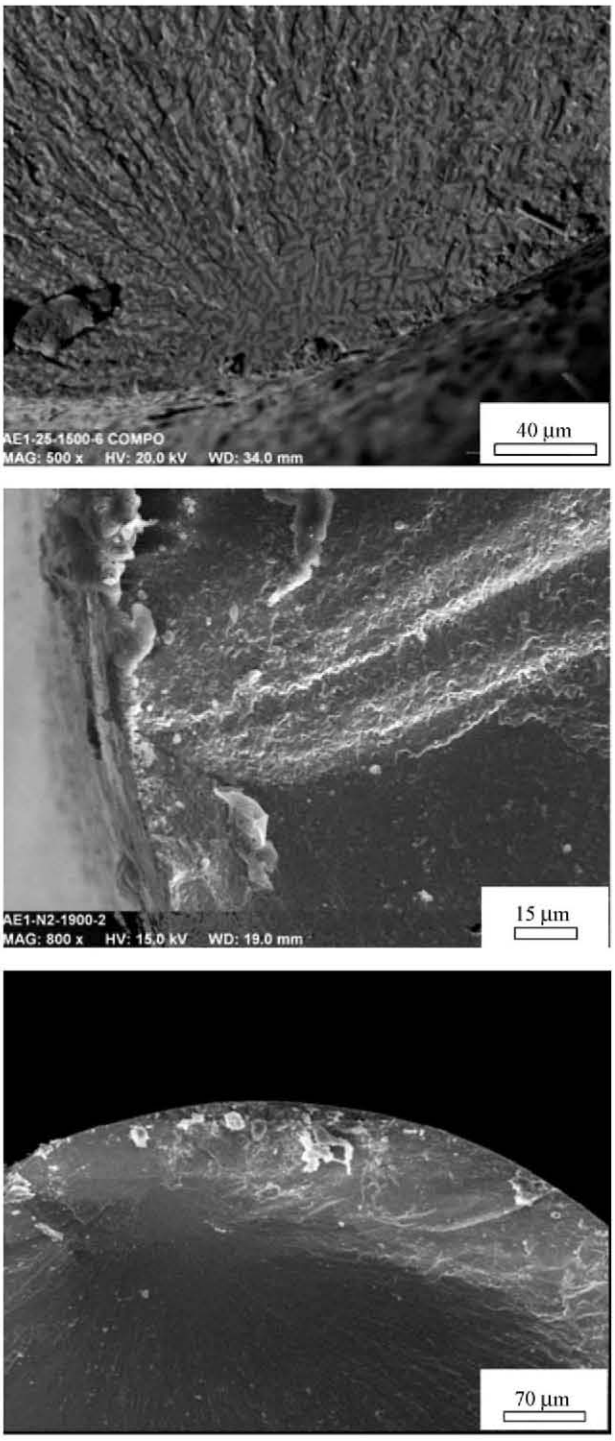

Fig. 10. Fracture initiation sites in Al_2O_3–$Er_3Al_5O_{12}$ eutectic rods. (a) Rod grown at 25 mm/h and tested at 300 K. (b) Rod grown at 350 mm/h and tested at 1900 K. (c) Rod grown at 750 mm/h and tested at 1900 K.

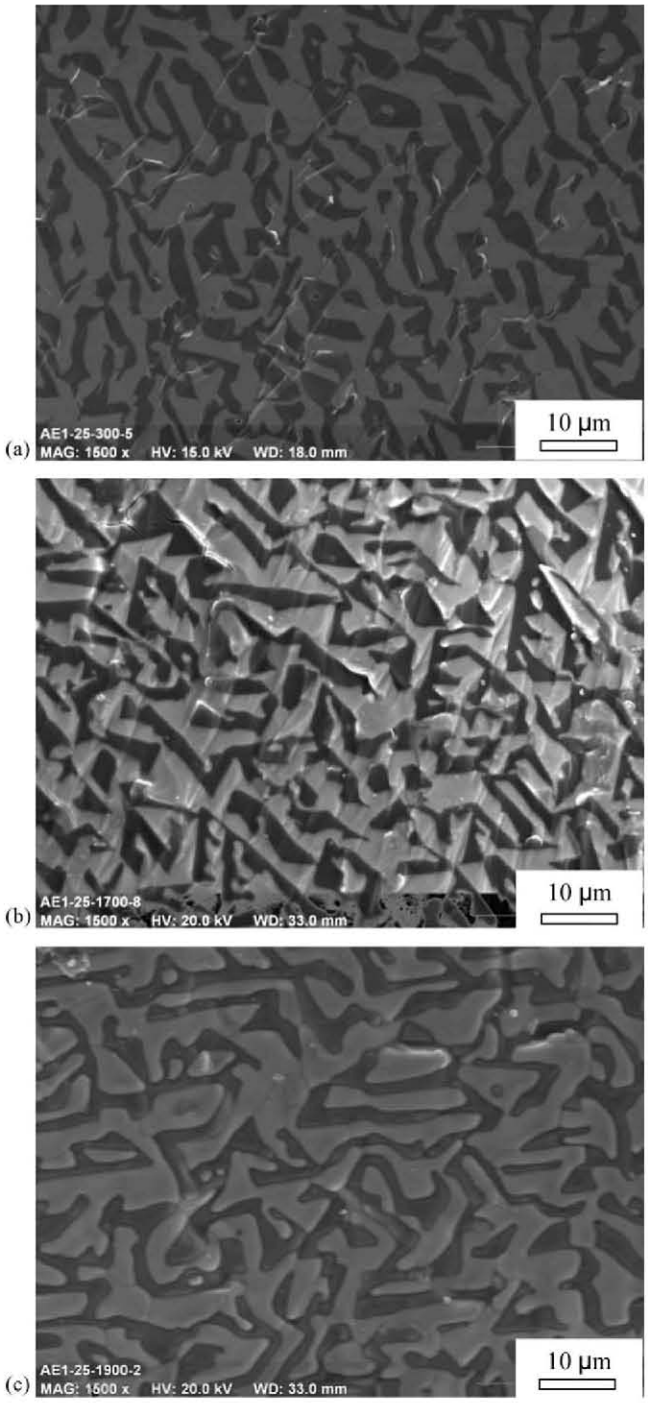

Fig. 11. Fracture surfaces of Al_2O_3–$Er_3Al_5O_{12}$ eutectic rods grown at 25 mm/h tested at (a) 300 K, (b) 1700 K and (c) 1900 K.

The bending strength of the rods as a function of temperature was determined from flexure tests at 300, 1300, 1500, 1700, and 1900 K. A minimum of three tests were carried for each material and temperature, and the average values (together with the corresponding standard errors) are plotted in Fig. 9. The strength of the Al_2O_3–$Er_3Al_5O_{12}$ eutectics grown at 25 and 350 mm/h remained practically constant up to 1300 K, while the eutectic with the finest microstructure showed an important reduction in strength at 1300 K. The three materials experienced a noticeable reduction in strength at higher temperatures, which reached a maximum in the eutectic grown at 750 mm/h. It is interesting to compare these results with those reported by Pastor et al.[4] in Al_2O_3–YAG rods grown at the same rates. While the ambient temperature strength of Al_2O_3–YAG was lower than that of Al_2O_3–EAG (Fig. 7), the strength retention at high temperature of Al_2O_3–YAG was significantly better and, as a result,

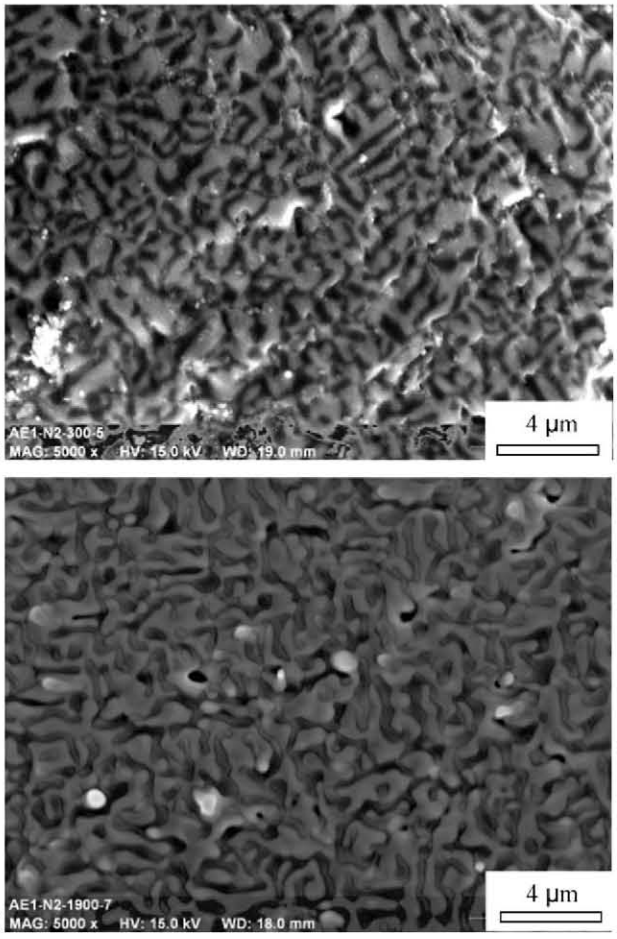

Fig. 12. Fracture surface of Al_2O_3–$Er_3Al_5O_{12}$ eutectic rods grown at 350 mm/h tested at (a) 300 K and (b) 1900 K.

the bending strength of eutectics of both materials grown at the same rate were very similar at 1900 K.

The fracture initiation site for each material and temperature was determined by means of a detailed analysis of the fracture surfaces in the scanning electron microscope. No differences were found between samples broken between 300 and 1900 K: fracture always began from surface defects, which could be easily traced from the river line patterns (Fig. 10). The fracture mechanisms of the samples broken at all temperatures always showed evidence of the same pattern: transgranular brittle fracture with very little evidence of damage accumulation before failure (Figs. 11–13). However, the analysis of the fracture surfaces showed changes with temperature, which also depended on interlamellar spacing.

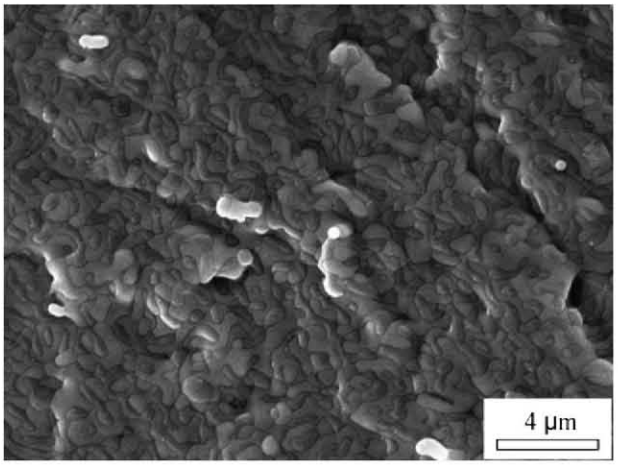

Fig. 13. Fracture surface of Al_2O_3–$Er_3Al_5O_{12}$ eutectic rods grown at 750 mm/h tested at 1900 K.

The fracture surface at 300 K of the eutectic grown at 25 mm/h (Fig. 11a) was flat, indicating that the crack propagated along a straight path without deflecting at interfaces or other defects. Although macroscopically flat, the fracture surface at 1700 K was rougher at microscopic level (Fig. 11b) and this may be due to the appearance of plastic deformation. Al_2O_3 and $Er_3Al_5O_{12}$ have different resistance to creep but the deformation of each phase was constrained by the interpenetrated microstructure. This leads to the development of stress concentrations along the plastic slip planes and at the interfaces, which interacted with the crack and gave rise to the microroughness observed in Fig. 11b. Finally, short-term exposure at 1900 K ($0.90T_m$) was enough to promote homogeneous coarsening of the microstructure and rounding of the faceted domains throughout the rod, as is shown in the fracture surface of the specimen tested at 1900 K (Fig. 11c).

Microstructure coarsening and rounding of the faceted domains was also seen on the fracture surfaces of the eutectics with finer microstructure tested at 1900 K (Figs. 12 and 13). The microroughness of the fracture surfaces was higher and, in addition, voids at the interfaces were seen throughout the fracture surfaces, indicating that the stress concentrations at the interfaces induced by the incompatibility in the plastic deformation of both phases was enough to promote interface voids.

The reduction in the bending strength at high temperature in the Al_2O_3–$Er_3Al_5O_{12}$ eutetic rods can be rationalized from the deformation and damage mechanisms observed in the fracture surfaces. Coarsening of the eutectic microstructure could be the source of strength degradation with temperature in these eutectics. As expected, the coarsening is significantly larger in the samples with the finest microstructure, leading to a rapid drop of the strength in the eutectic grown at 750 mm/h. In addition to this mechanism, the eutectics with finer microstructure grown at 350 and 750 mm/h also showed the development of interfacial voids. These voids and defects could act as crack-nucleation sites and contribute to reducing the strength at high temperature.

4. Conclusions

Al_2O_3–$Er_3Al_5O_{12}$ eutectic rods were processed by directional solidification using the laser-heated floating zone method at growth rates in the 25–1500 mm/h range. Rods grown up to 750 mm/h presented a homogeneous microstructure made up of an interpenetrating network of Al_2O_3 and $Er_3Al_5O_{12}$ phases. At higher growth rates, the interpenetrated microstructure coexisted with a fibrous pattern of Al_2O_3 fibers embedded in an $Er_3Al_5O_{12}$ matrix. Interphase spacing decreased with growth rate, following the Hunt–Jackson law $\lambda^2 v = C$, with $C = 135\ \mu m^3\ s^{-1}$. Thermo-elastic stresses developed in the eutectic upon cooling from the melt. Piezo-spectrocopic measurements showed that

Al_2O_3 was subjected to a hydrostatic stress of −135 MPa, which was independent of the interphase spacing.

Hardness and fracture toughness at room temperature was determined from the Vickers indentation test. Hardness increased slightly with growth rate, as was expected from the microstructural refinement, up to a maximum of 16 GPa. The fracture toughness was low (1.9 MPa $m^{1/2}$) and independent of the growth rate, and this brittle behaviour was supported by the fracture mechanisms: crack propagation was transgranular and fracture surfaces were flat.

The bending strength of the eutectic rods scaled linearly with $\lambda^{-1/2}$ because it was controlled by the critical size of the surface defects which depended on the interphase spacing. In addition, the homogeneity of the microstructure led to a very high bending strength, which attained 2.7 GPa in rods grown at 750 mm/h. This strength remained constant up to 1300 K and decreased at higher temperatures. Strength degradation above 1300 K was attributed to the homogeneous coarsening of the microstructure due to high-temperature exposure and to the nucleation of voids at the interface in the rods with finer microstructure.

Acknowledgements

This study was funded by the Ministry of Science and Innovation under projects MAT 2006-13005, MAT2007-29278-E, MAT 2009-13979 and ISOOC-06-1410, by the European Union under the project NMP4-SL-2008-213669 and by the Regional Government of Madrid under the ESTRUMAT-CM Programme (S-0505/MAT/0077). M.C. Mesa would like to thank the Gobierno de Aragón for a grant.

References

1. LLorca J, Orera VM. Directionally-solidified eutectic ceramic oxides. *Prog Mater Sci* 2006;**51**:711–809.
2. Waku Y, Nakagawa N, Wakamoto T, Ohtshubo H, Shimizu K, Kohtoku Y. High-temperature strength and thermal stability of a unidirectionally solidified Al_2O_3/YAG eutectic composite. *J Mater Sci* 1998;**33**: 1217–25.
3. Parthasarathy TA, Mah T-I, Matson LE. Deformation behavior of an $Al_2O_3/Y_3Al_5O_{12}$ eutectic composite in comparison with sapphire and YAG. *J Am Ceram Soc* 1993;**76**:29–32.
4. Pastor JY, LLorca J, Salazar A, Oliete PB, de Francisco I, Peña JI. Mechanical properties of melt-grown alumina–yttrium aluminum garnet eutectics up to 1900 K. *J Am Ceram Soc* 2005;**88**:1488–95.
5. Ramírez-Rico J, Pinto-Gómez AR, Martínez-Fernández J, de Arellano-López AR, Oliete PB, Peña JI, et al. High-temperature plastic behaviour of Al_2O_3–$Y_3Al_5O_{12}$ directionally solidified eutectics. *Acta Mater* 2006;**54**:3107–16.
6. Peña JI, Larsson M, Merino RI, de Francisco I, Orera VM, LLorca J, et al. Processing, microstructure and mechanical properties of directionally-solidified Al_2O_3–$Y_3Al_5O_{12}$–ZrO_2 ternary eutectics. *J Eur Ceram Soc* 2006;**26**:3113–21.
7. Oliete PB, Peña JI, Larrea A, Orera VM, LLorca J, Pastor JY, et al. Ultra-high strength nanofibrillar Al_2O_3–YAG–YSZ eutectics. *Adv Mater* 2007;**19**:2313–8.
8. Yoshikawa A, Hasegawa K, Lee JH, Durbin SD, Epelbaum BM, Yoon DH, et al. Phase identification of $Al_2O_3/RE_3Al_5O_{12}$ and $Al_2O_3/REAlO_3$ (RE = Sm–Lu, Y) eutectics. *J Cryst Growth* 2000;**218**:67–73.
9. Mazerolles L, Perriere L, Larigue-Korinec S, Piquet N, Parlier M. Microstructures, crystallography of interfaces and creep behaviour of melt-growth composites. *J Eur Ceram Soc* 2008;**28**:2301–8.
10. Perrière L, Valle R, Mazzerolles L, Parlier M. Crack propagation in directionally solidified eutectic ceramics. *J Eur Ceram Soc* 2008;**28**: 2337–43.
11. Chubb DL, Pal AT, Patton MO, Jenkins PP. Rare earth doped high temperature ceramic selective emitters. *J Eur Ceram Soc* 1999;**19**:2551–62.
12. Nakagawa N, Ohtsubo H, Waku Y, Yugami H. Thermal emission properties el $Al_2O_3/Er_3Al_5O_{12}$ eutectic ceramics. *J Eur Ceram Soc* 2005;**25**:1285–91.
13. Waku Y, Sakata S, Mitani A, Shimizu K, Ohtsubo H, Hasebe M. Microstructure and high-temperature strength of $Al_2O_3/Er_3Al_5O_{12}/ZrO_2$ ternary melt growth composite. *J Mater Sci* 2005;**40**:711–7.
14. Martínez-Fernández J, Sayir A, Farmer SC. High temperature creep deformation of directionally solidified $Al_2O_3/Er_3Al_5O_{12}$. *Acta Mater* 2003;**51**:1705–20.
15. Mizuno M. Phase diagrams of the systems Al_2O_3–Ho_2O_3 and Al_2O_3–Er_2O_3. *Yogyo Kyokai Shi* 1979;**87**:405–12.
16. Oliete PB, Peña JI. Study of the gas inclusions in $Al_2O_3/Y_3Al_5O_{12}$ and $Al_2O_3/Y_3Al_5O_{12}/ZrO_2$ eutectic fibers grown by laser floating zone. *J Cryst Growth* 2007;**304**:514–9.
17. Orera VM, Merino RI, Pardo JA, Larrea A, Peña JI, González C, et al. Microstructure and physical properties of some oxide eutectic crystals processed by directional solidification. *Acta Mater* 2000;**48**:4683–9.
18. Su H, Zhang J, Deng Y, Liu L, Fu H. A modified preparation technique and characterization of directionally solidified $Al_2O_3/Y_3Al_5O_{12}$ eutectic in situ composites. *Scr Mater* 2009;**60**:362–5.
19. Andreeta ERM, Andreeta MRB, Hernandes AC. Laser heated pedestal growth of $Al_2O_3/GdAlO_3$ eutectic fibers. *J Cryst Growth* 2002;**234**:782–5.
20. Saito M. Gas-bubble formation of ruby single crystals by floating zone method with an infrared radiation convergence type heater. *J Cryst Growth* 1985;**71**:664–72.
21. Elliot R. *Eutectic Solidification, Review 219, International Metals Reviews*; 1977. pp. 161–186.
22. Jackson KA, Hunt JD. Lamellar and rod eutectic growth. *Trans Metal Soc AIME* 1966;**236**:1129–42.
23. Epelbaum BM, Yoshikawa A, Shimamura K, Fukuda T, Suzuki K, Waku Y. Microstructure of $Al_2O_3/Y_3Al_5O_{12}$ eutectic rods grown by μ-PD method. *J Cryst Growth* 1999;**198/199**:471–5.
24. LLorca J, Pastor JY, Poza P, Peña JI, de Francisco I, Larrea A, et al. Influence of the Y_2O_3 content and temperature on the mechanical properties of melt-grown Al_2O_3–ZrO_2 eutectics. *J Am Ceram Soc* 2004;**87**:633–9.
25. Ciacchi LC, Gregori G, Lughi V, Rossi A, Sergo V. Piezo-spectroscopy: a materials science perspective. *Rec Res Devel Appl Spectrosc* 1999;**2**:243–72.
26. Harlan NR, Merino RI, Peña JI, Orera VM, González C, Poza P, et al. Phase distribution and residual stresses in melt-grown Al_2O_3–$ZrO_2(Y_2O_3)$ eutectics. *J Am Ceram Soc* 2002;**85**:2025–32.
27. Gupta YM, Shen XA. Potential use of the ruby R2 line shift for static high-pressure calibration. *Appl Phys Lett* 1991;**58**:583–5.
28. He J, Clarke DR. Determination of the piezospectroscopic coefficients for chromium-doped sapphire. *J Am Ceram Soc* 1995;**78**:1347–53.
29. Orera VM, Cemborain R, Merino RI, Peña JI, Larrea A. Piezo-spectroscopy at low temperatures: residual stresses in Al_2O_3–$ZrO_2(Y_2O_3)$ eutectics measured from 77 to 350 K. *Acta Mater* 2002;**50**:4677–86.
30. Ovanesyan KL, Petrosyan AG, Shirinyan GO, Avetisyan AA. Optical dispersion and thermal expansion of garnets $Lu_3Al_5O_{12}$, $Er_3Al_5O_{12}$ and $Y_3Al_5O_{12}$. *Inorg Mater* 1981;**17**:308–10.
31. Larrea A, Orera VM, Merino RI, Peña JI. Microstructure and mechanical properties of Al_2O_3–YSZ and Al_2O_3–YAG directionally solidified eutectic plates. *J Eur Ceram Soc* 2005;**25**:1419–29.
32. Lee JH, Yoshikawa A, Fukuda T, Waku Y. Microstructure of Y_2O_3 doped Al_2O_3–ZrO_2 eutectic fibers grown by the micro-pulling-down method. *J Cryst Growth* 2001;**231**:179–85.
33. Pastor, J.Y., Fractura de Materiales Cerámicos Estructurales Avanzados. Ph. D. Thesis, Universidad Complutense de Madrid, Madrid, Spain; 1993.
34. Quinn GD, Bradt RC. On the vickers indentation fracture toughness test. *J Am Ceram Soc* 2007;**90**:673–80.

35. Su H, Zhang J, Cui C, Liu L, Fu H. Rapid solidification of $Al_2O_3/Y_3Al_5O_{12}/ZrO_2$ eutectics in situ composites by laser zone remelting. *J Cryst Growth* 2007;**307**:448–56.
36. Anstis GR, Chantikul P, Lawn BR, Marshall DB. A critical evaluation of indentation techniques for measuring fracture toughness: I direct crack measurements. *J Am Ceram Soc* 1981;**64**:533–8.
37. Niihara K, Morena R, Hasselman DPH. Evaluation of K_{IC} of brittle solids by the indentation method with low crack-to-indent ratios. *J Mater Sci Lett* 1982;**1**:13–6.
38. Yang JM, Jeng SM, Chang S. Fracture behaviour of directionally solidified $Y_3Al_5O_{12}/Al_2O_3$ eutectic fiber. *J Am Ceram Soc* 1996;**79**: 1218–22.
39. Waku Y, Nakagawa N, Ohtsubo H, Mitani A, Shimizu K. Fracture and deformation behavior of melt-grown composites at very high temperature. *J Mater Sci* 2001;**36**:1594–5.
40. Newman JC, Raju IS. An empirical stress intensity factor equation for the surface crack. *Eng Fract Mech* 1981;**15**:185–92.